LPCVD growth of wide bandgap semiconductor In_2O_3 films

Md Rezaul Karim[1], Zixuan Feng[1] and Hongping Zhao[1,2‡]

[1]Department of Electrical and Computer Engineering, The Ohio State University, Columbus, OH 43210, USA

[2]Department of Materials Science and Engineering, The Ohio State University, Columbus, OH 43210, USA

‡ Email: zhao.2592@osu.edu

Abstract

Wide-bandgap semiconductor indium sesquioxide (In_2O_3) thin films were grown on yttria-stabilized-zirconia (YSZ) substrates with (100), (110) and (111) orientations using a previously unexplored growth method: low pressure chemical vapor deposition (LPCVD). High purity metallic indium (In) and oxygen (O_2) were used as precursors, and argon (Ar) was used as carrier gas. The growth condition was optimized to balance the precursor vapor pressure and the suppression of the gas phase reaction to facilitate the growth of high crystalline quality In_2O_3 films. The crystal structures of the as-grown films were determined to be body centered cubic bixbyite. By tuning the O_2 flow rate, In_2O_3 epitaxial growth rates of 21 μm/hour, 11 μm/hour and 9.2 μm/hour were obtained for films grown on YSZ (100), (110) and (111) substrates. Representative surface roughness values determined by atomic force microscopy ranges between 0.73-10.5 nm. Room temperature electron Hall mobility of 139 $cm^2/V{\cdot}s$, 77 $cm^2/V{\cdot}s$ and 97 $cm^2/V{\cdot}s$ for (100), (110), and (111) oriented In_2O_3 films were obtained with electron concentrations of ~$1.0\text{-}1.3x10^{18}$ cm^{-3}. Secondary Ion Mass Spectroscopy suggests H as a possible contributor to the observed free carrier concentrations in the as grown films. Room temperature photoluminescence peak was observed at ~ 2.16 eV, which is related to the transition involving deep-level defects. Optical bandgap was determined to be ~3.35-3.41 eV via photoluminescence excitation spectroscopy.

Keywords: Indium oxide, low pressure chemical vapor deposition (LPCVD), zirconia substrate

1. Introduction

Indium sesquioxide (In_2O_3) is a semiconducting oxide with fundamental bandgap of $E_g \sim 2.9$ eV, and optical bandgap of $E_{op} \sim 3.7$ eV[1]. In_2O_3 has been found to be inherently n-type due to the presence of oxygen vacancies and/or indium interstitials[2]. Hydrogen (H) has also been proposed as a potential shallow donor in as-grown In_2O_3[3-5]. The most stable phase of In_2O_3 is body center cubic (bcc) bixbyite structure, whereas corundum like rhombohedral (rh) phase can also be stabilized at high pressure and high temperature[6]. In_2O_3 was commonly used as a transparent conductive oxide as well as gas sensing material. Only recently, In_2O_3 has been investigated as a true semiconductor material and used as active semiconductor material for field effect transistors[7]. Moreover, alloying or heterostructure of In_2O_3 with group-III sesquioxides Ga_2O_3 ($E_g \sim 4.9$ eV) and Al_2O_3 ($E_g \sim 9$ eV) will provide new opportunities of bandgap engineering for electronic and optoelectronic device applications[8].

Essential for semiconductor device performance is the availability of high crystalline quality material with smooth surface morphology and reasonable growth rate[9]. Bulk single crystalline In_2O_3 has been synthesized by melt[10,11] and flux[12] growth techniques. Thin film In_2O_3 has been reported to be grown by pulsed laser deposition (PLD)[13,14], molecular beam epitaxy (MBE)[15-16], metalorganic chemical vapor deposition (MOCVD)[17], mist-chemical vapor deposition (mist-CVD)[8] and halide vapor phase epitaxy (HVPE)[9] methods. Epitaxial In_2O_3 films have been grown on yttria stabilized zirconia (YSZ)[15,16], sapphire[18] and most recently on Ga_2O_3 substrates[9]. Since single crystalline In_2O_3 substrates are not commercially available, YSZ substrates have been used as the best lattice-matched substrate (1.3 % lattice mismatch between 2x2 YSZ and 1x1 In_2O_3 unit cells) for epitaxy of In_2O_3 films[2].

To date the reported fastest growth rate (5.1 μm/hour) of In_2O_3 epitaxial layer was obtained by HVPE; however, the as-grown film surfaces were rough with the prevalence of pyramidal structures[9]. Epitaxial In_2O_3 films grown via MBE typically have growth rates of ~ 0.72 μm/hour[18] and MOCVD growth of In_2O_3 reported a growth rate of ~0.072 μm/hour[19]. Electron Hall mobility of ~190 $cm^2/V \cdot s$ and ~150 $cm^2/V \cdot s$ were achieved for as-grown unintentionally doped (UID) In_2O_3 films on YSZ (100) and YSZ (111) substrates via MBE[2,18]. However, the electron mobilities of UID In_2O_3 films grown by other techniques were typically lower than the reported bulk mobility (180 $cm^2/V \cdot s$)[10]. For instance, in case of bcc In_2O_3, electron Hall mobility of ~28 $cm^2/V \cdot s$[19] in MOCVD grown film on (100) YSZ, 110 $cm^2/V \cdot s$ in PLD grown film on (111) YSZ[14], and 16 $cm^2/V \cdot s$ and ~23 $cm^2/V \cdot s$ in HVPE grown films on (001) β-Ga_2O_3 and (0001) Al_2O_3 substrates[9] have been reported.

Low pressure chemical vapor deposition (LPCVD) technique has been recently demonstrated as a feasible approach to produce high quality β-Ga_2O_3 thin films on both native and foreign substrates, with controllable n-type doping and fast growth rates[20-24]. High purity metal and oxygen were used as the precursors and Ar was used as the carrier gas. The growth temperature and pressure were optimized by considering the balance between the precursor vapor pressure and the gas phase reaction.

In this work, for the first time, we report the growth of bcc-In_2O_3 thin film on YSZ substrates with (100), (110) and (111) crystal orientations by LPCVD. The effects of O_2 flow rate on the film growth rate, unintentional doping level and electron Hall mobility were investigated. Continuous In_2O_3 films with smooth surface morphology were achieved with growth rates as fast as 21

μm/hour, 11 μm/hour and 9.2 μm/hour on (100), (110) and (111) YSZ substrates, respectively. Under the current investigated growth conditions for In_2O_3 grown on YSZ substrates, electron Hall mobilities of 139 $cm^2/V{\cdot}s$, 77 $cm^2/V{\cdot}s$ and 97 $cm^2/V{\cdot}s$ were obtained on (100), (110) and (111) YSZ substrates with measured electron concentration of $1.24x10^{18}$ cm^{-3}, $1x10^{18}$ cm^{-3}, and $1.3x10^{18}$ cm^{-3}, respectively. H was identified as one of the possible contributors to the unintentional doping in the as grown films by Secondary Ion Mass Spectroscopy. Optical properties of the as-grown In_2O_3 films were investigated by photoluminescence (PL) and PL excitation (PLE) spectroscopy. The PL peak at ~ 2.16 eV was observed in In_2O_3 films grown on YSZ substrates, whereas PLE peaks occur at 3.35 eV, 3.38 eV and 3.41 eV, respectively, for (100), (110) and (111) oriented In_2O_3 films.

2. Experimental Section

In_2O_3 films were grown on (100), (110) and (111) oriented YSZ substrates in a custom-built tube furnace with programmable temperature and pressure controller. High purity In (Alfa Aesar, 99.998%) and O_2 (5N purity) were used as source materials whereas argon (Ar) was used as the carrier gas. The metal source was placed in a quartz crucible inside the tube furnace in such a way that the substrates were at a horizontally downstream location with respect to it. Prior to loading into the growth chamber, the substrates were sequentially cleaned with acetone and isopropanol, rinsed with deionized water and blow dried using nitrogen. The growth temperature was set as 950 °C. Five sets of samples were grown for 30 minutes with fixed Ar flow rate of 300 sccm and varied O_2 flow rate of 10, 15, 20, 25 and 30 sccm.

The crystal structures and crystalline qualities of the as-grown In_2O_3 films were evaluated by X-ray diffraction spectroscopy (XRD) using Bruker D8 Discover XRD. The surface morphology and roughness were characterized by field emission scanning electron microscopy (FESEM) using Helios Nanolab 600 and atomic force microscopy (AFM) using Bruker Icon 3. Film thicknesses were determined from cross-sectional FESEM images. The carrier transport properties were characterized by room temperature Van-der-Pauw Hall measurement using Ecopia HMS-3000 Hall effect measurement system. Room temperature PL and PLE spectroscopy were performed using Horiba Fluorolog 3 system equipped with high power continuous wavelength Xenon lamp.

3. Results and Discussion

XRD spectroscopy was performed to determine the crystalline structures of the as-grown In_2O_3 films. Figures 1a,c,e plot the 2θ-ω scan profiles for In_2O_3 films grown on (100), (110) and (111) oriented YSZ substrates. The observed diffraction peaks confirmed that the In_2O_3 films have bcc crystal structure with identical out-of-plane orientations as those of the YSZ substrates, i.e., In_2O_3 films were grown along [100], [110] and [111] directions on YSZ (100), (110) and (111) substrates, respectively. The 2θ-ω peaks exclusively correspond to the {200}, {220} and {222} plane families of the bcc-In_2O_3 films grown on YSZ (100), (110) and (111) substrates. The absence of any 2θ-ω peaks corresponding to rh-In_2O_3 crystal planes suggests phase purity in the as-grown films. To further evaluate the crystalline quality of the In_2O_3 films, ω-rocking curves around the (400), (440) and (222) XRD peaks were measured from the same set of samples, as shown in Figures 1b,d,f. The full width at half maxima (FWHM) of the diffraction peaks are 299 arcsec, 308 arcsec and 358 arcsec, respectively. The FWHM values of these LPCVD grown In_2O_3 films are narrower than those reported previously. For example, 396 arcsec FWHM of In_2O_3 (400) peak was reported for

an MBE grown film[18], and 756 arcsec FWHM of In_2O_3 (222) peak was reported for an MOCVD grown film[19] on YSZ substrate.

Figure 2 shows the XRD Φ-scan profiles of off-axis (222), (400) and (440) planes obtained from (100), (110) and (111) oriented In_2O_3 films, respectively. For (100) In_2O_3 film, four (222) peaks separated by $\Delta\Phi = 90^{\circ}$ have been observed (Figure 2a), which indicate four-fold rotational symmetry of (222) planes along [100] direction. Similar Φ-scan profiles of off-axis (222) planes in (100) oriented bixbyite YSZ have been reported in literature[25]. On the other hand, two-fold rotational symmetry of (110) In_2O_3 surfaces[26] are evident from two off-axis (400) peaks in Φ-scan profile of (110) In_2O_3 film as shown in Figure 2b. For In_2O_3 film with (111) orientation, as can be seen from Figure 2c, three off-axis (440) peaks ($\Delta\Phi \sim 120^{\circ}$) were observed in Φ-scan profile. This is consistent with three-fold rotational symmetry of (111) In_2O_3 surfaces. Therefore, XRD Φ-scan profiles reveal the absence of rotational domains in the In_2O_3 films being reported here.

Figures 3a,b,c represent the cross-sectional FESEM images of the as-grown In_2O_3 films on YSZ (100), (110) and (111) substrates, respectively. As indicated in the figures, the thicknesses of the films are 10.5 μm, 5.5 μm and 4.6 μm. The corresponding growth rates for the films are 21 μm/hour, 11 μm/hour, and 9.2 μm/hour, respectively. Figure 4 plots the In_2O_3 growth rates on YSZ (100), (110) and (111) substrates as a function of the O_2/Ar flow rate ratio. For each growth orientation, the growth rate can be affected and controlled by various growth parameters including the growth temperature, growth pressure, precursor flow rates and ratio. Under the same growth condition, the observed different growth rate for In_2O_3 films grown on zirconia substrates with different crystal orientation can be due to several possible factors including the substrate surface energy, surface morphology, defects such as dislocations intersecting the surface, and

unintentional wafer miscut[23,27]. From Figure 4, the epitaxial In_2O_3 growth rate increases with increase of the O_2/Ar ratio up to a certain value beyond which the growth rate decreases with further increase in the O_2/Ar ratio. Under the investigated conditions, the fastest growth rates of 21 μm/hour (on (100) YSZ substrate), 11 μm/hour (on (100) YSZ substrate) and 9.2 μm/hour (on (111) YSZ substrate) were obtained with O_2/Ar flow rate ratio of 0.05. We believe that the In_2O_3 films were grown in In-rich condition and therefore, increase in O_2 flow rate increases the growth rate. The observed reduction in growth rate with further increase in O_2/Ar ratio beyond the peak value can be attributed to the reduced In vapor due to the increased vapor phase reaction of precursors[28].

As shown in Figure 5, both FESEM and AFM were used to characterize the surface morphology of the as-grown In_2O_3 films on YSZ (100), (110) and (111) substrates. The continuous In_2O_3 film grown on YSZ (100) substrate (Figure 5a) has a relatively flat surface although with the presence of steps. The average height of the steps is ~0.5 nm. The RMS determined from AFM scanning over 3 μm x 3 μm area is 2.53 nm (Figure 5d). For the In_2O_3 film grown on YSZ (110) substrate, the SEM image (Figure 5b) shows the surface having corrugated morphology with [-110] being the direction of corrugation. The corresponding AFM image (Figure 5e) shows the RMS of 10.5 nm. To identify the orientation of the corrugated side facets on the (110) In_2O_3 surface, we estimated the angle δ between the sidewall and substrate surface via the AFM line scan as shown in Figure 5f. The δ angle was estimated to be ~ 35° from the relatively prominent groove structures. Therefore, the side facet is determined to be {111} orientated. Corrugated In_2O_3 (110) surface with {111} or {100} oriented side facets have also been observed in case of MBE growth under moderately In-rich condition[26]. Relative surface energies (γ) of low indexed In_2O_3 surfaces have

been experimentally shown to be $\gamma(111) < \gamma(100) < \gamma(110)$. However, it has been predicted that in highly In-rich condition, $\gamma(110)$ may become smaller than $\gamma(100)$ and $\gamma(111)$ [26]. The facet control of LPCVD growth of In_2O_3 (110) films still require further studies. In case of the In_2O_3 film grown on YSZ (111) substrate, the surface of the as-grown film is featureless at the scale used in the FESEM image as shown in Figure 5c. The corresponding AFM image in Figure 5g reveals the atomic step of 0.2 nm and RMS of 0.73 nm. Overall, the surface morphologies suggest continuous In_2O_3 films were grown on YSZ substrates with all three investigates orientations. The surface morphologies are smooth considering the fast growth rates for these films.

Room temperature Van-der-Pauw Hall measurements were performed to characterize the carrier concentrations and carrier mobilities for the as-grown UID In_2O_3 films. Figures 6a,b plot the measured carrier concentrations and Hall mobilities in In_2O_3 films grown with different O_2/Ar ratio. The measured electron concentrations in (100), (110) and (111) oriented films vary in the range of 1.8-7.4x10^{18} cm^{-3}, 1.0-5.1x10^{18} cm^{-3} and 1.3-9.8x10^{18} cm^{-3}, respectively. The corresponding mobility values range from 68-97 $cm^2/V{\cdot}s$, 65-77 $cm^2/V{\cdot}s$ and 42-97 $cm^2/V{\cdot}s$, respectively. Besides, for (100) oriented In_2O_3 films, electron Hall mobility of 139 $cm^2/V{\cdot}s$ was achieved with further tuning of the growth condition. Within the range of the measured Hall electron concentrations, the mobility values have been described in literature to be limited by scattering due to polar optical phonons[29]. However, detailed investigation of transport mechanisms requires temperature dependent Hall measurements as part of our future works.

As indicated in Figure 6, both electron concentration and Hall mobility are highly dependent on the O_2/Ar flow rate ratio. In general, the electron concentration initially decreases with increase in

O_2/Ar ratio, reaching a minimum value, and then increases with further increase in O_2/Ar ratio. The mobilities show the opposite trend as expected that the highest mobility values occurred in the films with the lowest electron concentrations for all three In_2O_3 films grown on YSZ substrates. However, the free carrier concentrations in the films grown with O_2/Ar flow rate ratio of 2.5/30 show deviations from the general trend. As reported previously, the unintentional doping in In_2O_3 films has been ascribed to various mechanisms including the incorporation of impurities, for example, hydrogen from the growth environment and native point defects (oxygen vacancies and/or In interstitials)[2-5]. In both cases, the observed deviation may arise from several factors including non-uniformity of the substrate and surface preparation. To better understand the origin of background electron concentration in LPCVD grown In_2O_3 films, Secondary Ion Mass Spectroscopy (SIMS) was performed on differently oriented In_2O_3 films grown with O_2/Ar flow rate ratio of 2.5/30. Figure 7 presents the measured SIMS depth profiles of H and C obtained from In_2O_3 (100), (110) and (111) films. From Figure 7a, we observe significant incorporation of H impurity in all the samples, particularly, within the top 300-500 nm region. Moreover, H concentration in the (111) oriented film is substantially higher than those in (110) and (100) oriented films, which is consistent with the free carrier concentration results obtained by Hall measurement (Figure 6). On the other hand, as shown in Figure 7b, C incorporation is not significant in any of the samples. Based on these measurements, H can serve as a possible contributor to the unintentional electron concentrations in LPCVD grown In_2O_3 films. However, H incorporation does not discard native point defects as another source of free carriers in the as-grown In_2O_3 films. Further investigation including both experiment and theory are still required to obtain the complete picture.

In order to investigate the optical properties of different oriented In_2O_3 epitaxial layers, room temperature PL and PLE spectroscopy were performed. Near band-edge emission peak is typically not observable in PL spectra for In_2O_3 films[2]. Theoretical calculations suggest that the transition from valence band maxima (VBM) to the conduction band minima (CBM) is dipole forbidden[30,31] and the VBM is slightly shifted from the CBM at Γ-point rendering the bandgap to be slightly indirect[32]. Moreover, in literature the onset of weak absorption around the fundamental bandgap has been attributed to weak forbidden direct transition[31], phonon-assisted indirect transition or combination of both[32]. On the other hand, PLE spectroscopy has been used as a technique to measure the absorption edge of semiconductor materials[33,34]. Figure 8 plots the PL and PLE spectra of the as-grown In_2O_3 films grown on (100), (110) and (111) YSZ substrates. The excitation wavelength of 400 nm was used for the PL spectra measurements, and the PL peak appeared at ~ 2.16 eV (575 nm), which is consistent with the greenish-yellow appearance of the samples. The PL peak energy is substantially lower than that of the fundamental or optical band gap energy of In_2O_3[1]. Such below band gap emissions from cubic In_2O_3 has been ascribed to the radiative recombination involving deep level defect states created by oxygen vacancies[2,35]. On the other hand, the PLE spectra, which were collected for emission wavelength of 575 nm, show the absorption peaks at 3.35 eV, 3.38 eV and 3.41 eV for (100), (110) and (111) oriented In_2O_3 films, respectively. These values are in good agreement with the theoretically predicted optical band gap of In_2O_3 films[30]. The Hall carrier concentrations of these samples are 1.24×10^{18} cm^{-3}, 1.7×10^{18} cm^{-3} and 2.14×10^{18} cm^{-3}, respectively. Within the parabolic dispersion approximation, Moss-Burstein shifts at these concentrations[36] are not sufficient to account for the observed variation between the obtained optical bandgaps in (100), (110) and (111) In_2O_3 films. However, actual band structure

of In_2O_3 is much more complicated[37,38] and to probe the fundamental properties will require both experimental and theoretical investigations.

The demonstrated LPCVD growth of single crystalline In_2O_3 films with fast growth rates, smooth surface morphology, and reasonable carrier transport properties will promote its potential as a wide bandgap semiconductor material for device applications. With our previously developed LPCVD growth of β-Ga_2O_3, it is promising to develop In_2O_3/Ga_2O_3 alloys and heterostructures for high performance electronic and optoelectronic devices.

4. Conclusion

In summary, In_2O_3 thin films were grown on (100), (110) and (111) YSZ substrates via LPCVD using high purity metallic In and O_2 gas as precursors. XRD spectroscopy has revealed the grown films are single crystalline with bcc crystal structure. By tuning the O_2 flow rate, In_2O_3 film growth rates of 21 μm/hour, 11 μm/hour and 9.2 μm/hour were achieved for the films grown on YSZ (100), (110) and (111) substrates. Room temperature Hall mobility of 139 $cm^2/V{\cdot}s$, 77 $cm^2/V{\cdot}s$ and 97 $cm^2/V{\cdot}s$ were obtained with carrier concentrations in the range of 1-2x10^{18} cm^{-3}. Obvious H incorporation was determined from SIMS depth profile, which can contribute to the observed free carriers in the as grown In_2O_3 films. PL peak was observed at ~ 2.16 eV for each type of films due to transitions involving deep level defects. The measured PLE peaks at ~3.35-3.41 eV agree with the theoretically predicted optical band gap of In_2O_3. The investigation of LPCVD growth and transport properties of In_2O_3 as a true semiconductor material will pave a new way for its potential application in electronic and optoelectronic devices.

Acknowledgements

The authors acknowledge the funding support from the National Science Foundation (DMR-1755479).

References

(1) King, P. D. C.; Veal, T. D.; Fuchs, F.; Wang, C. Y.; Payne, D. J.; Bourlange, A.; Zhang, H.; Bell, G. R.; Cimalla, V.; Ambacher, O.; Egdell, R. G.; Bechstedt, F.;McConville, C. F. Band gap, electronic structure, and surface electron accumulation of cubic and rhombohedral In_2O_3. *Phys. Rev. B* 2009, 79, 205211.

(2) Bierwagen, O. Indium oxide - a transparent, wide-band gap semiconductor for (opto)electronic applications. *Semicond. Sci. Technol*. 2015, 30, 024001.

(3) Koida, T.; Fujiwara, T.; Kondo, M. Hydrogen-doped In_2O_3 as high-mobility transparent conductive oxide. *Jpn. J. Appl. Phys.* 2007, 46, L685–L687.

(4) Limpijumnong, S.; Reunchan, P; Janotti, A.; Van de Walle, C. G. Hydrogen doping in indium oxide: An *ab initio* study. *Phys. Rev. B* 2009, 80, 193202.

(5) King, P. D. C.; Lichti, R. L.; Celebi, Y. G.; Gil, J. M.; Vilão, R. C.; Alberto, H. V.; Duarte, J. P.; Payne, D. J.; Egdell, R. G.; McKenzie, I.; McConville, C. F.; Cox, S. F. J.; Veal, T. D. Shallow donor state of hydrogen in In_2O_3 and SnO_2: Implications for conductivity in transparent conducting oxides. *Phys. Rev. B* 2009, 80, 081201(R).

(6) Karazhanov, S. Z.; Ravindran, P.; Vajeeston, P.; Ulyashin, A.; Finstad T. G.; Fjellvåg H. Phase stability, electronic structure, and optical properties of indium oxide polytypes. *Phys. Rev. B* 2007, 76, 075129.

(7) Kaneko, K.; Ito, Y.; Uchida, T.; Fujita, S. Growth and metal-oxide-semiconductor field-effect transistors of corundum-structured alpha indium oxide semiconductors. *Appl. Phys. Express* 2015, 8, 095503.

(8) Fujita, S.; Kaneko, K. Epitaxial growth of corundum-structured wide band gap III-oxide semiconductor thin films. *J. Cryst. Growth* 2014, 401, 588-592.

(9) Togashi, R.; Numata, S.; Hayashida, M.; Suga, T.; Goto, K.; Kuramata, A.; Yamakoshi, S.; Paskov, P.; Monemar, B.; Kumagai, Y. High rate growth of In_2O_3 at 1000 °C by halide vapor phase epitaxy. *Jpn. J. Appl. Phys.* 2016, 55, 1202B3.

(10) Galazka, Z.; Uecker, R.; Irmscher, K.; Schulz, D.; Klimm, D.; Albrecht, M.; Pietsch, M.; Ganschow, S.; Kwasniewski, A.; Fornari, R. Melt growth, characterization and properties of bulk In_2O_3 single crystals. *J. Cryst. Growth* 2013, 362, 349-352.

(11) Galazka, Z.; Uecker, R.; Fornari, R. A novel crystal growth technique from the melt: Levitation-assisted self-seeding crystal growth method. *J. Cryst. Growth* 2014, 388, 61-69.

(12). Hagleitner, D. R.; Menhart, M.; Jacobson, P.; Blomberg, S.; Schulte, K.; Lundgren, E.; Kubicek, M.; Fleig, J.; Kubel, F.; Puls, C.; Limbeck, A.; Hutter, H.; Boatner, L. A.; Schmid, M.; Diebold, U. Bulk and surface characterization of In_2O_3(001) single crystals. *Phys. Rev. B* 2012, 85, 115441.

(13) Tarsa, E. J.; English, J. H.; Speck, J. S. Pulsed laser deposition of oriented In_2O_3 on (001) InAs, MgO, and yttria-stabilized zirconia. *Appl. Phys. Lett.* 1993, 62, 2332.

(14) Koida, T.; Kondo, M. High electron mobility of indium oxide grown on yttria-stabilized zirconia. *J. Appl. Phys.* 2006, 99, 123703.

(15) Bourlange, A.; Payne, D.; Palgrave, R.; Foord, J.; Egdell, R.; Jacobs, R.; Schertel, A.; Hutchison, J.; Dobson, P. Investigation of the growth of In_2O_3 on Y-stabilized ZrO_2(100) by oxygen plasma assisted molecular beam epitaxy. *Thin Solid Films* 2009, 517, 4286-4294.

(16) Bierwagen, O.; White, M. E.; Tsai, M.-Y.; Speck, J. S. Plasma-assisted molecular beam epitaxy of high quality In_2O_3(001) thin films on Y-stabilized ZrO_2(001) using In as an auto surfactant. *Appl. Phys. Lett.* 2009, 95, 262105.

(17) Wang, C. Y.; Kirste, L.; Morales, F. M.; Mànuel, J. M.; Röhlig, C. C.; Köhler, K.; Cimalla, V.; García, R.; Ambacher, O. Growth mechanism and electronic properties of epitaxial In_2O_3 films on sapphire. *J. Appl. Phys.* 2011, 110, 093712.

(18) Bierwagen, O.; Speck, J. S. Nucleation of islands and continuous high-quality In_2O_3(001) films during plasma-assisted molecular beam epitaxy on Y-stabilized ZrO_2(001). *Appl. Phys. Lett.* 2010, 97, 072103.

(19) Zhao, C.; Li, Z.; Mi, W.; Luan, C.; Feng, X; Ma, J. Structure and optical properties of epitaxial indium oxide films deposited on Y-stabilized ZrO_2(111) by MOCVD. *J. Electron. Mater.*, 44, 2719-2724.

(20) Rafique, S.; Han, L.; Zhao, H. Synthesis of wide bandgap Ga_2O_3 ($E_g \sim 4.6 – 4.7$ eV) thin films on sapphire by low pressure chemical vapor deposition. *Phys. Status Solidi A* 2016, 213, 1002-1009.

(21) Rafique, S.; Han, L.; Neal, A. T.; Mou, S.; Tadjer, M. J.; French, R. H.; Zhao, H. Heteroepitaxy of N-type β-Ga_2O_3 thin films on sapphire substrate by low pressure chemical vapor deposition. *Appl. Phys. Lett.* 2016, 109, 132103.

(22) Rafique, S.; Han, L.; Tadjer, M. J.; Freitas Jr., J. A.; Mahadik, N. A.; Zhao, H. Homoepitaxial growth of β-Ga_2O_3 thin films by low pressure chemical vapor deposition. *Appl. Phys. Lett.* 2016, 108, 182105.

(23) Rafique, S.; Han, L.; Neal, A. T.; Mou, S.; Boeck, J.; Zhao, H. Towards high-mobility heteroepitaxial β-Ga_2O_3 on sapphire - dependence on the substrate off-axis angle. *Phys. Status Solidi A* 2017, 215, 1700467.

(24) Rafique, S.; Karim, M. R.; Johnson, J. M.; Hwang, J.; Zhao, H. LPCVD homoepitaxy of Si doped β-Ga_2O_3 thin films on (010) and (001) substrates. *Appl. Phys. Lett.* 2018, 112, 05210423.

(25) Garcia, G.; Figueras, A.; Merino, R. I.; Orera, V. M.; Llibre, J. Structural and optical properties of yttria-stabilized-zirconia films grown by MOCVD. *Thin Solid Films* 2000, 370, 173 – 178.

(26) Bierwagen, O.; Rombach, J.; Speck, J. S. Faceting control by the stoichiometry influence on the surface free energy of low-index bcc-In_2O_3 surfaces. *J. Phys.: Condens. Matter* 2016, 28, 224006.

(27) Zhang, K. H. L.; Walsh, A.; Catlow, C. R. A.; Lazarov, V. K.; Egdell, R. G. Surface energies control the self-organization of oriented In_2O_3 nanostructures on cubic zirconia. *Nano Lett.* 2010, 10, 3740-3746.

(28) Kleijn, C.; Dorsman, R.; Kuijlaars, K. J.; Okkerse, M.; Santen, H. v. Multi-scale modeling of chemical vapor deposition processes for thin film technology. *J. Cryst. Growth* 2007, 303, 362-380.

(29) Preissler, N.; Bierwagen, O.; Ramu, A. T.; Speck, J. S. Electrical transport, electrothermal transport, and effective electron mass in single-crystalline In_2O_3 films. *Phys. Rev. B* 2013, 88, 085305.

(30) Walsh, A.; Da Silva, J. L. F.; Wei, S. H.; Körber, C.; Klein, A.; Piper, L. F. J.; DeMasi, A.; Smith, K. E.; Panaccione, G.; Torelli, P.; Payne, D. J.; Bourlange, A.; Egdell, R. G. Nature of the band gap of In_2O_3 revealed by first-principles calculations and X-ray spectroscopy. *Phys. Rev. Lett.* 2008, 100, 167402.

(31) Fuchs, F.; Bechstedt, F. Indium-oxide polymorphs from first principles: Quasiparticle electronic states. *Phys. Rev. B*, 77, 155107.

(32) Irmscher, K.; Naumann, M.; Pietsch, M.; Galazka, Z.; Uecker, R.; Schulz, T.; Schewski, R.; Albrecht, M.; Fornari, R. On the nature and temperature dependence of fundamental bandgap of In_2O_3. *Phys. Status Solidi A* 2014, 211, 54 – 58.

(33) Rafique, S.; Han, L.; Mou, S.; Zhao, H. Temperature and doping concentration dependence of the energy band gap in β-Ga_2O_3 thin films grown on sapphire. *Opt. Mater. Express* 2017, 7, 3561-3570.

(34) Lin, Z.; Zhu, Q.; Dong, Y.; Liu, S.; Li, J.-G.; Li, X.; Huo, D.; Zhang, M.; Xie, M.; Sun, X. Synthesis and formation mechanisms of morphology-controllable indium-containing precursors and optical properties of the derived In_2O_3 particles. *CrystEngComm*. 2016, 18, 3768-3776.

(35) Weiher, R. L.; Ley, R. P. Optical properties of indium oxide. *J. Appl. Phys.* 1966, 37, 299-302.

(36) Sato, Y.; Ashida, T.; Oka, N.; Shigesato, Y. Carrier density dependence of optical band gap and work function in Sn-doped In_2O_3 films. *Appl. Phys. Express* 2010, 3, 061101.

(37) Walsh, A.; Da Silva, J. L. F.; Wei, S.-H. Origins of band-gap renormalization in degenerately doped semiconductors. Phys. Rev. B. 2008, 78, 075211.

(38) Feneberg, M.; Nixdorf, J.; Lidig, C.; Goldhahn, R.; Galazka, Z.; Bierwagen, O.; Speck, J. S. Many-electron effects on the dielectric function of cubic In_2O_3: Effective electron mass, band nonparabolicity, band gap renormalization, and Burstein-Moss shift. *Phys. Rev. B* 2016, 93, 045203.

Figure Captions

Figure 1. XRD spectra of In_2O_3 films grown on YSZ substrates with different orientations. (a, c, e) 2θ-ω scan of In_2O_3 films grown on YSZ (100), (110) and (111) substrates, respectively. (b, d, f) ω-rocking curve of bcc-In_2O_3 (400), (440) and (222) peaks for films grown on YSZ (100), (110) and (111) substrates, respectively. The samples were grown with 2/30 O_2/Ar flow rate ratio.

Figure 2. XRD Φ-scan of off-axis bcc-In_2O_3 (a) (222), (b) (400), and (c) (440) planes obtained from In_2O_3 films grown on (100), (110) and (111) YSZ substrates, respectively. The samples were grown with O_2/Ar rate ratio of 2/30.

Figure 3. Cross-sectional FESEM images of In_2O_3 films grown on (a) (100), (b) (110) and (c) (111) oriented YSZ substrates. These samples were grown for 30 mins under the same growth condition with O_2/Ar flow rate ratio of 1.5/30.

Figure 4. The growth rates of In_2O_3 film on YSZ (100), (110) and (111) substrates as a function of the O_2/Ar flow rate ratio.

Figure 5. (a-c) Top-view FESEM and (d,e,g) 3 μm x 3 μm AFM images of as-grown In_2O_3 films on (100), (110) and (111) oriented YSZ substrates. (f) AFM scan profile of the (110) In_2O_3 film along the white dashed line marked in the inset. [-110] corrugation direction is marked by white arrows in b and e. The samples were grown with O_2/Ar flow rate ratio of 2/30.

Figure 6. (a) Electron concentration, and (b) Hall mobility in (100), (110) and (111) oriented In_2O_3 films grown with different O_2/Ar flow rate ratio.

Figure 7. SIMS depth profile of atomic (a) H and (b) C concentrations in (100), (110) and (111) In_2O_3 films. Detection limit is 10^{17} atoms/cm^3 for both impurity elements. The samples were grown with 2.5/30 O_2/Ar flow rate ratio. From cross-sectional SEM image, the thicknesses of (100), (110) and (111) oriented films are ~1.5 μm, ~1.1 μm and ~0.7 μm, respectively.

Figure 8. PL and PLE spectra of the as-grown In_2O_3 epitaxial films on YSZ (100), (110) and (111) oriented substrates. The samples were grown with O_2/Ar flow rate ratio of 2/30.

Figure 1

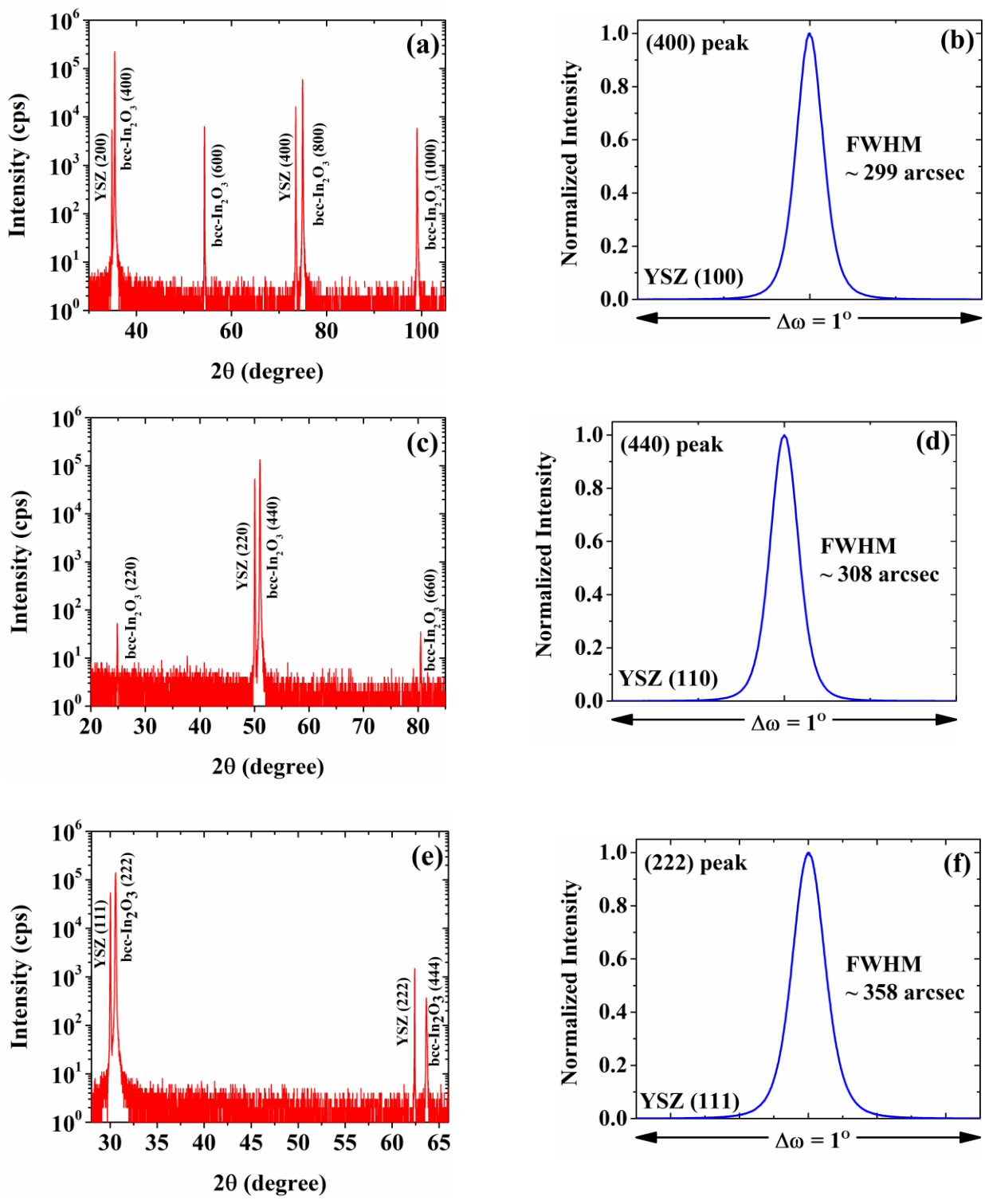
(a)
Intensity (cps)
2θ (degree)
YSZ (200)
bcc-In2O3 (400)
bcc-In2O3 (600)
YSZ (400)
bcc-In2O3 (800)
bcc-In2O3 (1000)
(b)
(400) peak
FWHM
~ 299 arcsec
YSZ (100)
Normalized Intensity
Δω = 1°
(c)
bcc-In2O3 (220)
YSZ (220)
bcc-In2O3 (440)
bcc-In2O3 (660)
(d)
(440) peak
FWHM
~ 308 arcsec
YSZ (110)
(e)
YSZ (111)
bcc-In2O3 (222)
YSZ (222)
bcc-In2O3 (444)
(f)
(222) peak
FWHM
~ 358 arcsec
YSZ (111)

Figure 2

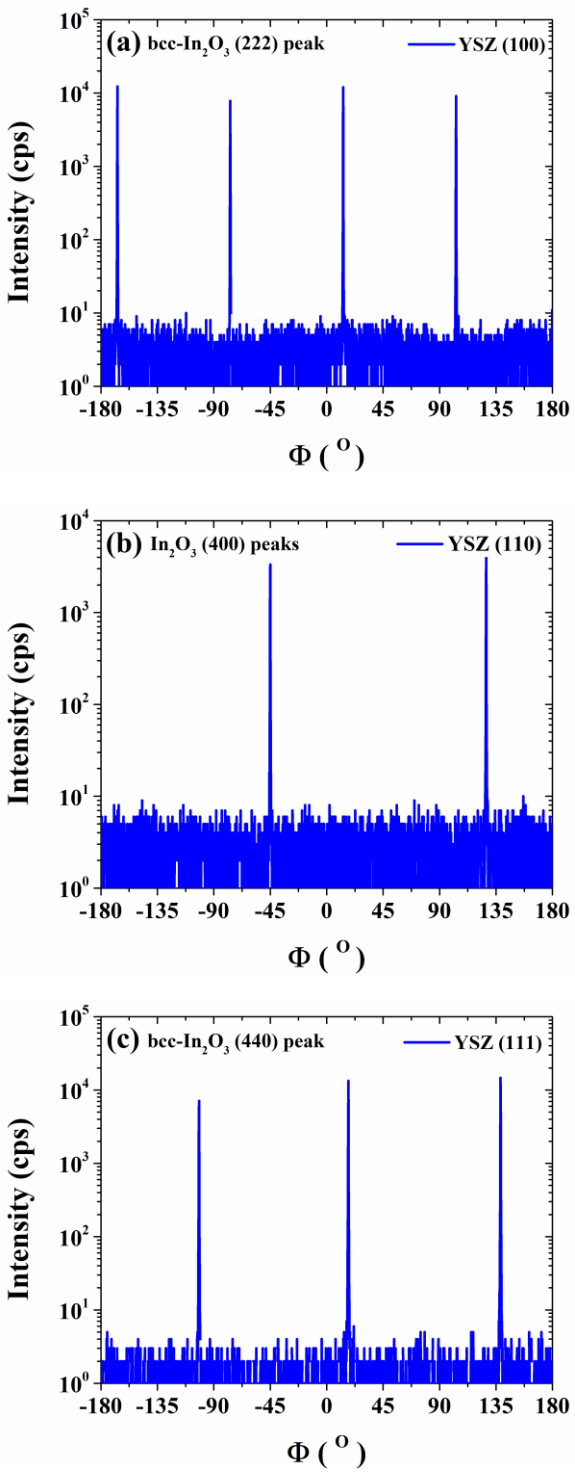
(a) bcc-In2O3 (222) peak
YSZ (100)
(b) In2O3 (400) peaks
YSZ (110)
(c) bcc-In2O3 (440) peak
YSZ (111)
Intensity (cps)
Φ (O)
-180 -135 -90 -45 0 45 90 135 180

Figure 3

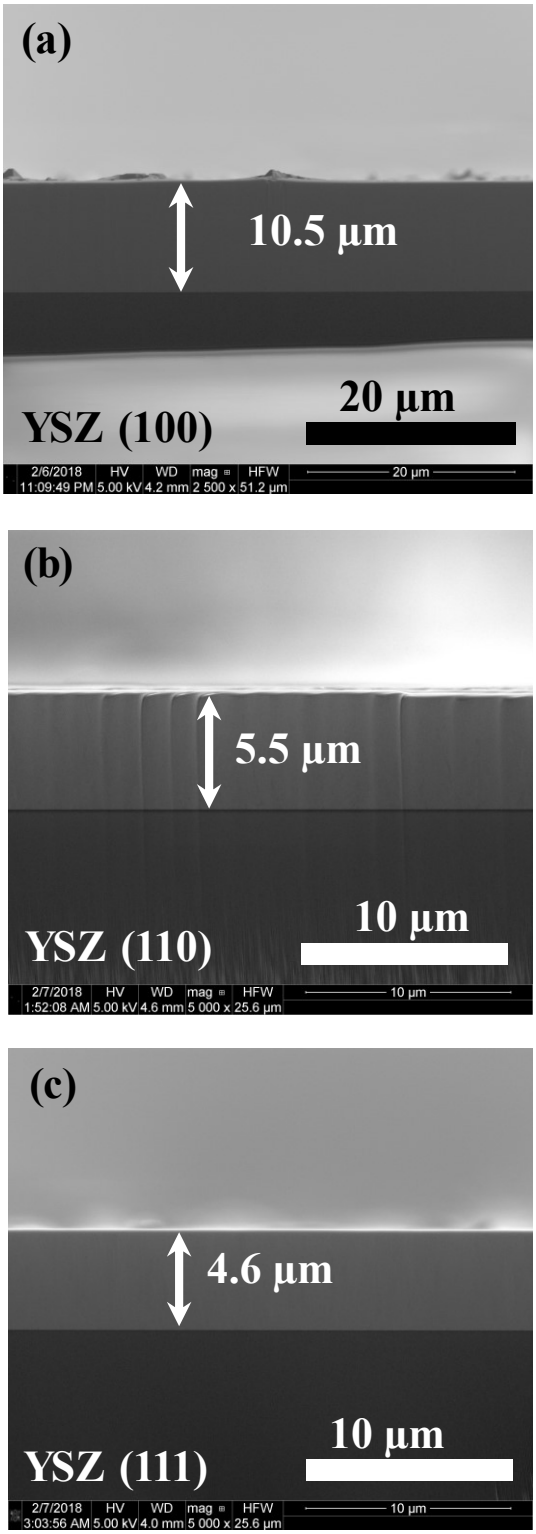
(a)
10.5 µm
20 µm
YSZ (100)
2/6/2018 HV WD mag HFW
11:09:49 PM 5.00 kV 4.2 mm 2 500 x 51.2 µm
20 µm
(b)
5.5 µm
10 µm
YSZ (110)
2/7/2018 HV WD mag HFW
1:52:08 AM 5.00 kV 4.6 mm 5 000 x 25.6 µm
10 µm
(c)
4.6 µm
10 µm
YSZ (111)
2/7/2018 HV WD mag HFW
3:03:56 AM 5.00 kV 4.0 mm 5 000 x 25.6 µm
10 µm

Figure 4

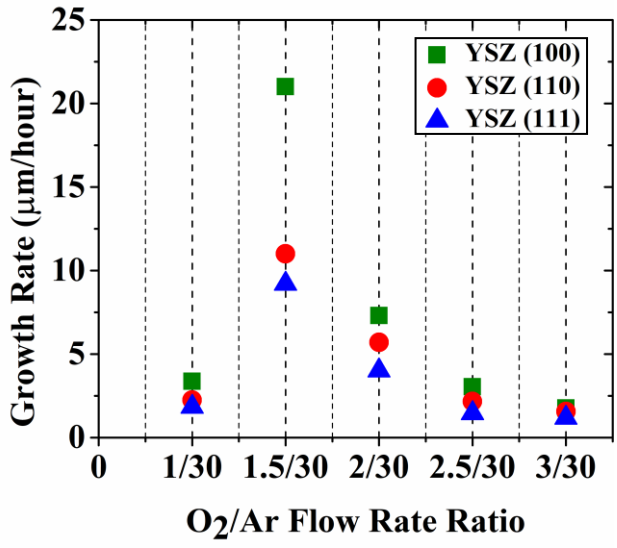
25
20
15
10
5
0
Growth Rate (μm/hour)
0
1/30
1.5/30
2/30
2.5/30
3/30
O2/Ar Flow Rate Ratio
YSZ (100)
YSZ (110)
YSZ (111)

Figure 5

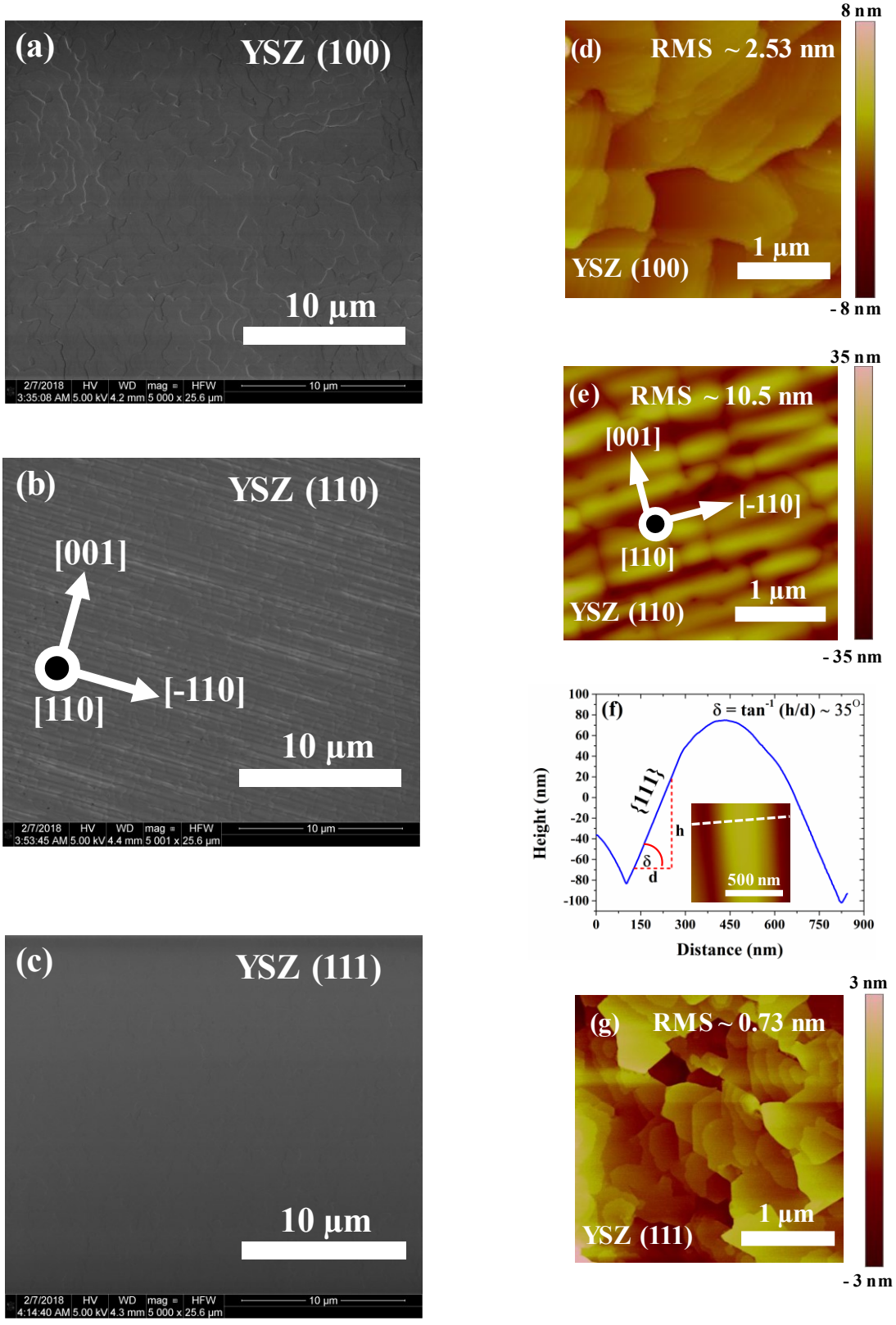
(a)
YSZ (100)
10 µm
2/7/2018 HV WD mag HFW
3:35:08 AM 5.00 kV 4.2 mm 5 000 x 25.6 µm
10 µm
(b)
YSZ (110)
[001]
[-110]
[110]
10 µm
2/7/2018 HV WD mag HFW
3:53:45 AM 5.00 kV 4.4 mm 5 001 x 25.6 µm
10 µm
(c)
YSZ (111)
10 µm
2/7/2018 HV WD mag HFW
4:14:40 AM 5.00 kV 4.3 mm 5 000 x 25.6 µm
10 µm
(d)
RMS ~ 2.53 nm
1 µm
YSZ (100)
8 nm
- 8 nm
(e)
RMS ~ 10.5 nm
[001]
[-110]
[110]
1 µm
YSZ (110)
35 nm
- 35 nm
(f)
δ = tan-1 (h/d) ~ 35O
{111}
h
δ
d
500 nm
Height (nm)
Distance (nm)
(g)
RMS ~ 0.73 nm
1 µm
YSZ (111)
3 nm
- 3 nm

Figure 6

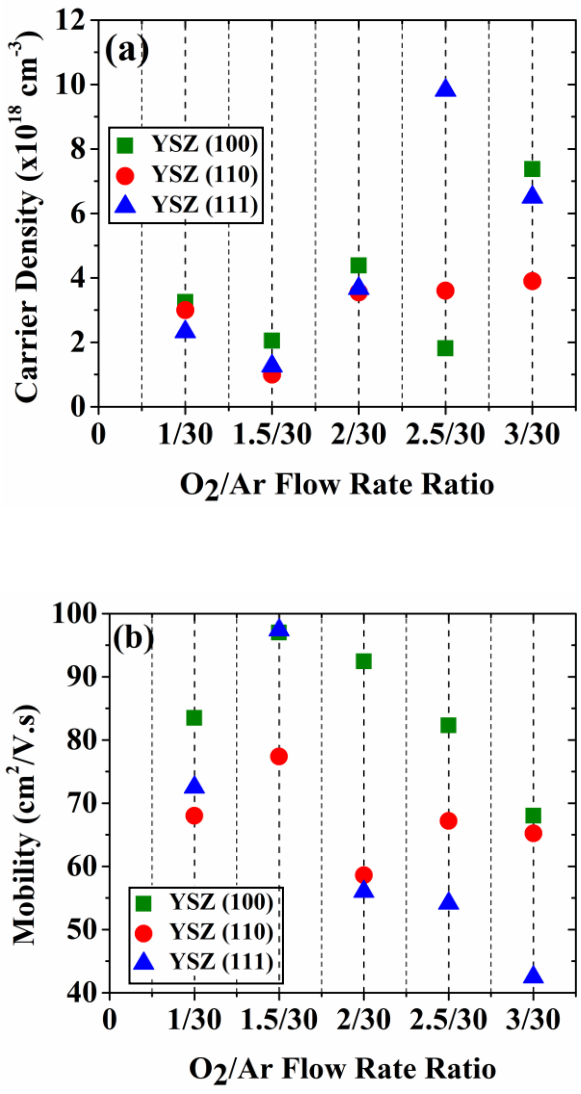
(a)
YSZ (100)
YSZ (110)
YSZ (111)
Carrier Density (x10^18 cm^-3)
0
2
4
6
8
10
12
0
1/30
1.5/30
2/30
2.5/30
3/30
O2/Ar Flow Rate Ratio
(b)
YSZ (100)
YSZ (110)
YSZ (111)
Mobility (cm^2/V.s)
40
50
60
70
80
90
100
0
1/30
1.5/30
2/30
2.5/30
3/30
O2/Ar Flow Rate Ratio

Figure 7

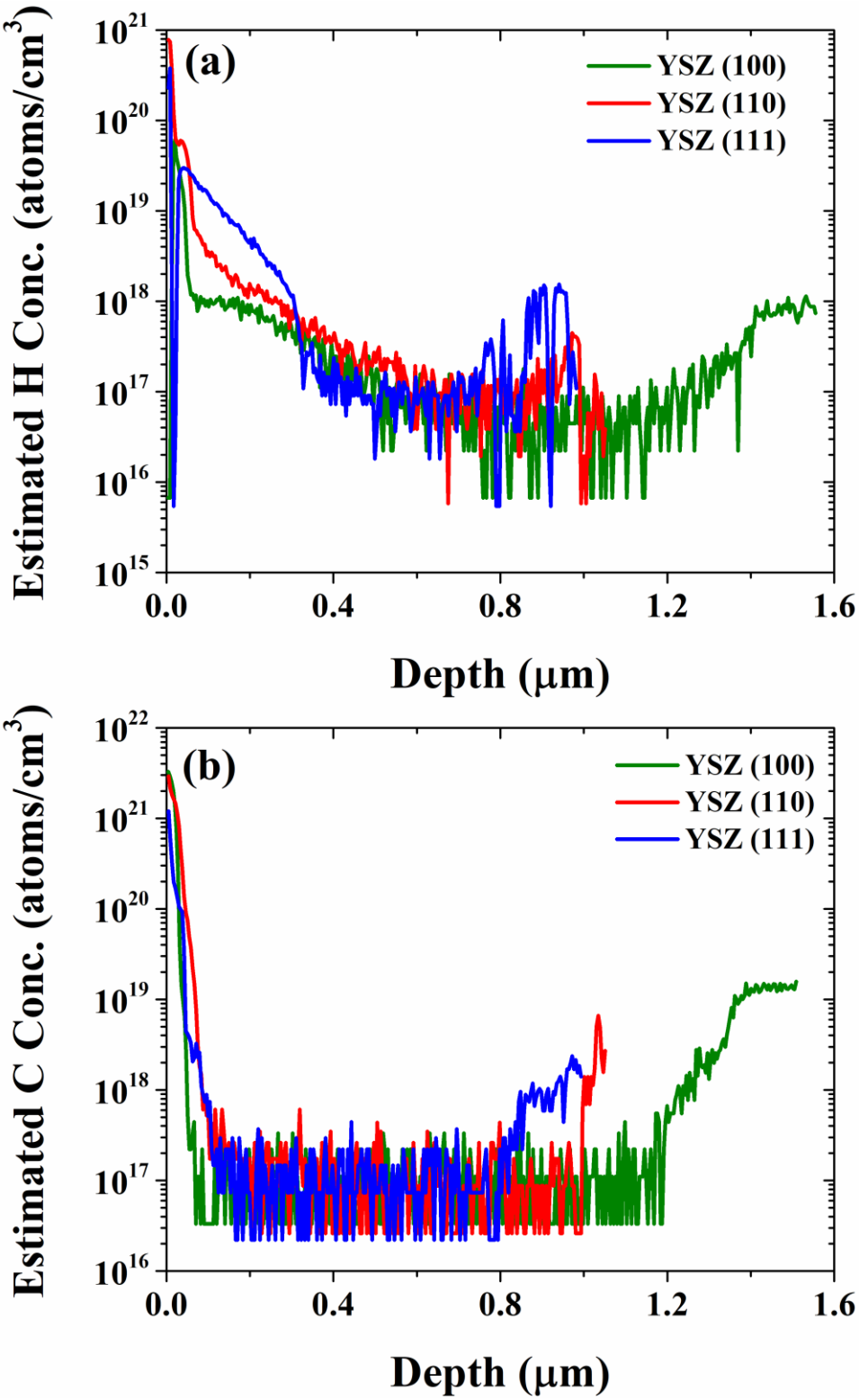
(a)
YSZ (100)
YSZ (110)
YSZ (111)
Estimated H Conc. (atoms/cm^3)
10^{21}
10^{20}
10^{19}
10^{18}
10^{17}
10^{16}
10^{15}
0.0
0.4
0.8
1.2
1.6
Depth (μm)
(b)
YSZ (100)
YSZ (110)
YSZ (111)
Estimated C Conc. (atoms/cm^3)
10^{22}
10^{21}
10^{20}
10^{19}
10^{18}
10^{17}
10^{16}
0.0
0.4
0.8
1.2
1.6
Depth (μm)

Figure 8

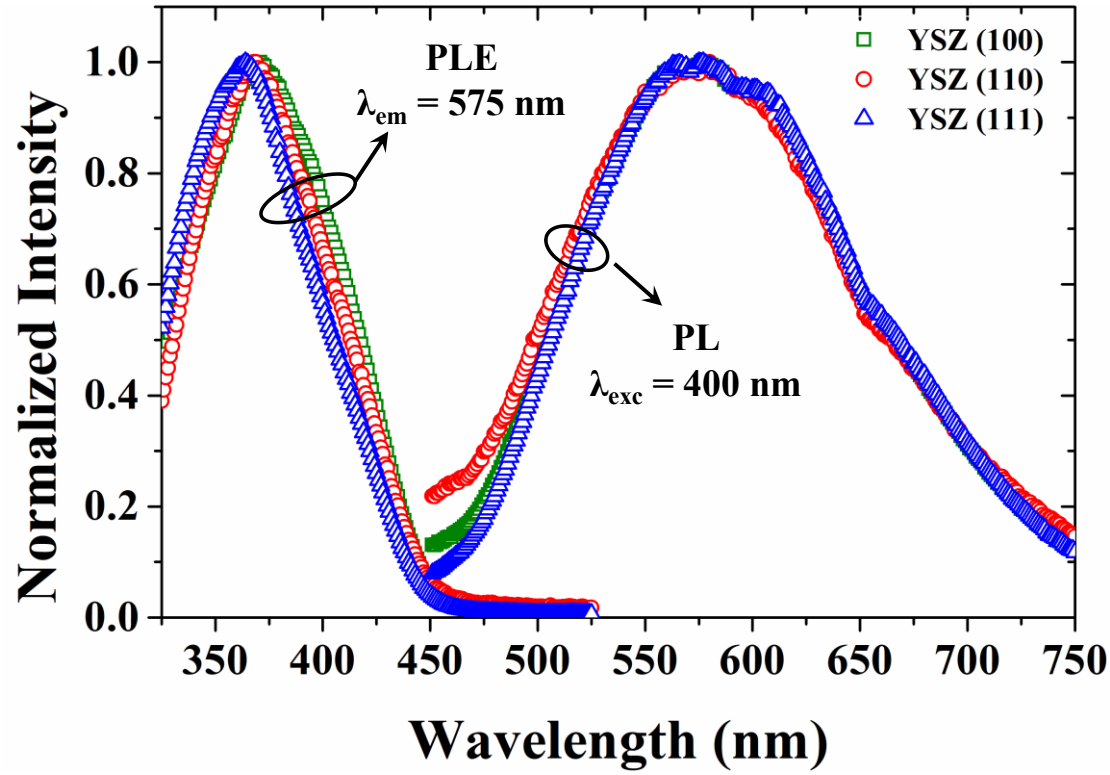
PLE
λ_{em} = 575 nm
PL
λ_{exc} = 400 nm
YSZ (100)
YSZ (110)
YSZ (111)
Normalized Intensity
Wavelength (nm)
0.0
0.2
0.4
0.6
0.8
1.0
350
400
450
500
550
600
650
700
750

For Table of Contents Use Only

LPCVD growth of wide bandgap semiconductor In_2O_3 films

Md Rezaul Karim[1], Zixuan Feng[1] and Hongping Zhao[1,2‡]

[1]Department of Electrical and Computer Engineering, The Ohio State University, Columbus, OH 43210, USA

[2]Department of Materials Science and Engineering, The Ohio State University, Columbus, OH 43210, USA

‡ Email: zhao.2592@osu.edu

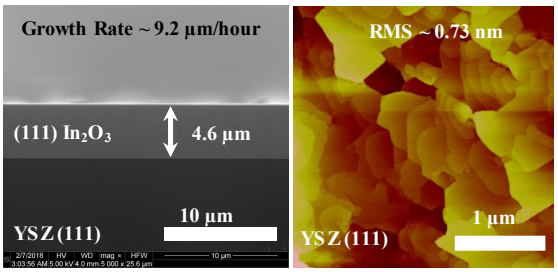

In_2O_3 thin films were grown on yttria stabilized zirconia substrates by low pressure chemical vapor deposition. Single crystalline films with bcc bixbyite crystal structures, smooth surfaces and promising transport properties were obtained at substantially faster growth rate than those reported previously. H was found to be a possible contributor to unintentional doping. The measured optical bandgaps agree with theoretical predictions.